Automatika

Journal for Control, Measurement, Electronics, Computing and Communications

ISSN: (Print) (Online) Journal homepage: https://www.tandfonline.com/loi/taut20

Inverter current control for reactive power compensation in solar grid system using Self-Tuned Fuzzy Logic Controller

R. Nirmala & S. Venkatesan

To cite this article: R. Nirmala & S. Venkatesan (2022) Inverter current control for reactive power compensation in solar grid system using Self-Tuned Fuzzy Logic Controller, Automatika, 63:1, 102-121, DOI: 10.1080/00051144.2021.2009653

To link to this article: https://doi.org/10.1080/00051144.2021.2009653

Published online: 29 Nov 2021.

AUTOMATIKA
2022, VOL. 63, NO. 1, 102–121
https://doi.org/10.1080/00051144.2021.2009653

Inverter current control for reactive power compensation in solar grid system using Self-Tuned Fuzzy Logic Controller

R. Nirmala and S. Venkatesan

Department of EEE, A.C. Government College of Engineering and Technology, Karaikudi, India

ABSTRACT

The solar photovoltaic (PV) systems have gained more attention in renewable energy production due to their cost efficiency and reliability. Typically, reactive power compensation and harmonics elimination are challenging and demanding tasks for improving the efficacy of grid-connected solar PV systems. For this purpose, many research works developed different converter and controller topologies for solving the power quality issues in grid-PV systems. But, it limits the problems of increased harmonics, computation complexity, inefficiency and reduced performance outcomes. Thus, this research aims to develop an integrated hysteresis current controller and Self-Tuned Fuzzy Logic (SFLC) based MPPT controllers for eliminating the harmonics and unbalanced current in single-phase grid systems. Also, it helps to extract the maximum amount of power from the solar PV array. The LUO converter is deployed to reduce ripple contents. The Phased Locked Loop (PLL) based synchronization is performed to maintain the phase angle, frequency and magnitude levels of source power. Moreover, the hysteresis current controller for the inverter has been specifically designed to reduce the THD of the system under IEEE519_1992 regulations. During experiments, both the simulation and hardware results have been evaluated for validating the performance of the proposed controller design.

ARTICLE HISTORY
Received 24 March 2021
Accepted 30 September 2021

KEYWORDS
Maximum Power Point Tracking (MPPT); photovoltaic (PV); grid connected; Self-Tuned Fuzzy Logic Controller (SFLC); reactive power compensation (RPC)

Nomenclature

μ_{sc}	The cell temperature coefficient (A/k)
a	Modified ideality factor
ADP	Approximate Dynamic Programming
ANN	Artificial Neural Network
APF	Active Power Filtering
DC	Direct Current
DTDPLL	Dual Transport Delay based Phase Lock Loop
FLC	Fuzzy Logical Controller
G	Irradiation (Watt/m^2)
G_{ref}	Irradiation at STC (Watt/m^2) = 1000 Watt/m^2
I_0	The diode reverse saturation current (A)
I_D	Diode current (A)
I_{ph}	Photo absorption current (A)
I_{pv}	Photovoltaic current (A)
I_{sc-ref}	The PV module reference short circuit current (A)
I_{sh}	Shunt current (A)
LCO-FLL	Limit Cycle Oscillator – Frequency Locked Loop
MPPT	Maximum Power Point Tracking
PCC	Predictive Current Control, Point of Common Coupling
PI	Proportional Integral
PV	Photovoltaic
RMS	Root Mean Square
R_P	Solar cell parallel resistance (ohm)
RPC	Reactive power compensation
R_S	Solar cell series resistance (ohm)
SAPF	Shunt Active Power Filter
SEPIC	Single-Ended Primary-Inductor Converter
SFLC	Self-Tuned Fuzzy Logic Controller
T_{ref}	Temperature at STC (K)
ΔT	T–T_{ref}. Where T = Temperature (Kelvin)

1. Introduction

In recent days, power demand has been drastically increased due to the rapid growth of population and industrialization. So, electricity generation [1] is one of the challenging tasks, and the source of generation is either renewable or non-renewable. When compared to non-renewable energy sources, renewable energy sources [2,3] have gained significant attention due to their cost efficiency and reliability, in which the solar photovoltaic (PV) [4,5] systems are considered as the best source for electricity generation and also it has been extensively used in many application areas. The significant benefits of using solar PV systems [6,7] are

CONTACT R. Nirmala nirmala21harsha@gmail.com

better maintenance, reduced cost, high efficiency and pollution free. Typically, the isolation and ambient temperature of the PV panels are unpredictable, because it has non-linear voltage and current characteristics. For this purpose, a Maximum Power Point Tracking (MPPT) controlling technique [8–12] is used to track the maximum power from the solar PV systems. In single-stage PV systems, the inner and outer loops are realized simultaneously for simplifying the system topology [13]. In the traditional works, there are different converter topologies that have been used in the PV system, which include buck, boost, buck–boost, CUK, LUO and SEPIC for solving the power quality problems. Still, the basic converters limit with some drawbacks like increased complexity and cost consumption, so some of the advanced converter topologies have been developed for the PV systems over the past decades. But, the selection of an appropriate converter is necessary to obtain the maximum utilization of the PV power; amongst all advanced converter topologies, the DC–DC LUO converter contains some inherent properties of higher converter efficiency, lower ripple content and higher voltage gain [14].

The incorporation of a reactive power compensation unit in a single-phase PV system can improve the overall performance of the grid system. Typically, reactive power compensation [15] and harmonics distortion elimination [16] are the most concentrated research problems in the domain of solar PV systems. Also, it can be characterized based on two ways such as voltage and load, and in both cases, the reactive power flow [17,18] must be controlled and compensated in an efficient way for better system performance. However, the filtering technique does not provide a competent compensation performance due to the simultaneous operations of varying loads. So, it is highly required to compensate the non-efficient components [19,20] such as unbalanced, harmonics and reactive in a grid system for increasing the filtering efficiency. Gayatri et al. [21] presented a detailed review of the reactive power compensation techniques for improving the efficacy of micro-grid systems. The primary consideration of this paper was to analyse the power quality issues that could affect the performance of grid systems and their corresponding compensation methodologies to resolve the problems. This study diagnosed that various controlling methods were used to provide an appropriate solution for reactive power compensation. Zhang et al. [22] suggested a unified controller strategy with a z-source converter for reactive power compensation in a solar PV system. Also, a Space Vector Pulse Width Modulation (SVPWM) technique was applied in a grid system for injecting a shoot-through duty. The main aim of this paper was to compensate for the reactive power and efficiently reduce the current harmonics. Ali et al. [23] examined the effectiveness of the reactive power compensation mechanism for the Cyprus distribution grid. This work suggested two possible solutions based on location and distance parameters to offer the required compensation.

Li et al. [24] recommended a controlling strategy for reactive power compensation in grid-connected PV systems. The main intention of this work was to improve the power quality and utilization rate of the PV inverters. Also, it aimed to reduce the voltage fluctuations and harmonic distortions using an optimization-based controlling algorithm. Moreover, it includes the controlling modes of cloudy mode, night mode, reverse power control and normal operation mode. These controlling operations were performed to reduce the voltage oscillations by maintaining the stability of the grid systems. Still, it is required to reduce the total harmonics distortion value for improving the performance of the entire grid system. Wang et al. [25] implemented a hybrid modulation method for performing a competent reactive power compensation using an H6 inverter. Here, different switching patterns were included for avoiding current distortions. Also, the relationship between the time setup and power factor was analysed based on the time intervals. The advantage of this technique was, it could be modified and adapted for any H6 inverter topologies. Pandey et al. [26] deployed a new controlling strategy named Limit Cycle Oscillator – Frequency Locked Loop (LCO-FLL) for reducing the load harmonics in a single-stage PV system. Also, a Proportional Integral (PI) controller was used to regulate the voltage under varying irradiance and load dynamics. Moreover, it aimed to reduce the burden of reactive power on the utility grid systems. The disadvantage behind this work was required to improve the overall performance of the power distribution systems. Bhole and Shah [27] employed a Predictive Current Control (PCC) methodology to solve power quality issues in grid-connected PV systems. This work mainly intends to compensate for the reactive power and reduce the total harmonics distortion using an Active Power Filtering (APF) technique. In addition, it was used to increase the system's power quality by reducing the neutral current and line current harmonics.

Beena et al. [28] presented a new control approach for enhancing the power quality of grid-interactive inverter. The major considerations of this work were to reduce the total harmonics distortions, injection of DC, power factor and voltage fluctuations. For grid synchronization, a Phase Locked Loop (PLL) technique was employed to ensure active and reactive power control. But, this work failed to concentrate on energy conservation for increasing the reliability of the power system. Chourasiya et al. [29] suggested a Fuzzy Logic Control (FLC) based SAPF technique for performing reactive power compensation with reduced harmonics distortion and settling time of DC voltage. Also, the PLL-based synchronization technique was utilized to maintain the phase angle and magnitude values.

Still, it is required to increase the effectiveness of the overall system by implementing an efficient controlling methodology.

To solve these problems, this research work intends to develop a compensation technique with advanced controller and converter topologies for reactive power compensation, harmonics removal and unbalanced current elimination. The objectives that have been mainly focused in the proposed work are as follows:

- To extract the maximum power from the solar PV systems with reduced computational complexity, a Self-Tuned Fuzzy Logic Controller (SFLC) technique is employed.
- To adeptly maintain the constant voltage and eliminate the ripple contents, the DC–DC LUO converter topology is utilized.
- To eliminate the harmonics and unbalanced current in a grid system, the hysteresis current controller and Self-Tuned MPPT Fuzzy Controller have been integrated. It also compensates reactive power in the proposed system.

The remaining sections of this paper are organized as follows: proposed SFLC-based Reactive Power Compensation System is presented in Section 2. The LUO converter analysis is shown in Section 3. The detection and compensation of reactive power are explained in Section 4 and the result analysis is shown in Section 5. Then, its corresponding outcomes are depicted in Section 6. Finally, the overall paper is concluded with its future scope in Section 7.

2. Proposed SFLC-based reactive power compensation system

Figure 1 shows the block representation of the proposed reactive power compensation system, where voltage and current of a PV system are interdependent, for a given value of irradiation and temperature, there is only one value of the load at which maximum power is extracted from the PV system. The DC–DC LUO converter used in this design comprises the following benefits: low output voltage ripples, easier compensation and good performance characteristics. Here, the voltage levels V_{pv} are controlled by the LUO converter with a stable dc-link voltage. The MPPT controller produces the reference PV current I_{ref} and their reference gate pulses to the converters are generated by using the hysteresis controller method. The reference current consists of two components such as (i) real power component (I_P*) that corresponds to the maximum power to be injected and (ii) reactive power component (I_Q*) that could be I_P* at 90°. In inverter side current controller RPC, the maximum possible reactive power injection I_Q* can be determined as follows:

$$|I_Q^*|^2 = |I^*|^2 - |I_P^*|^2 \tag{1}$$

where I_P* is the RMS value of real power component of i_s*; I_Q* is the RMS value of reactive power component of i_s*; $I*$ is the RMS value of inverter rated current.

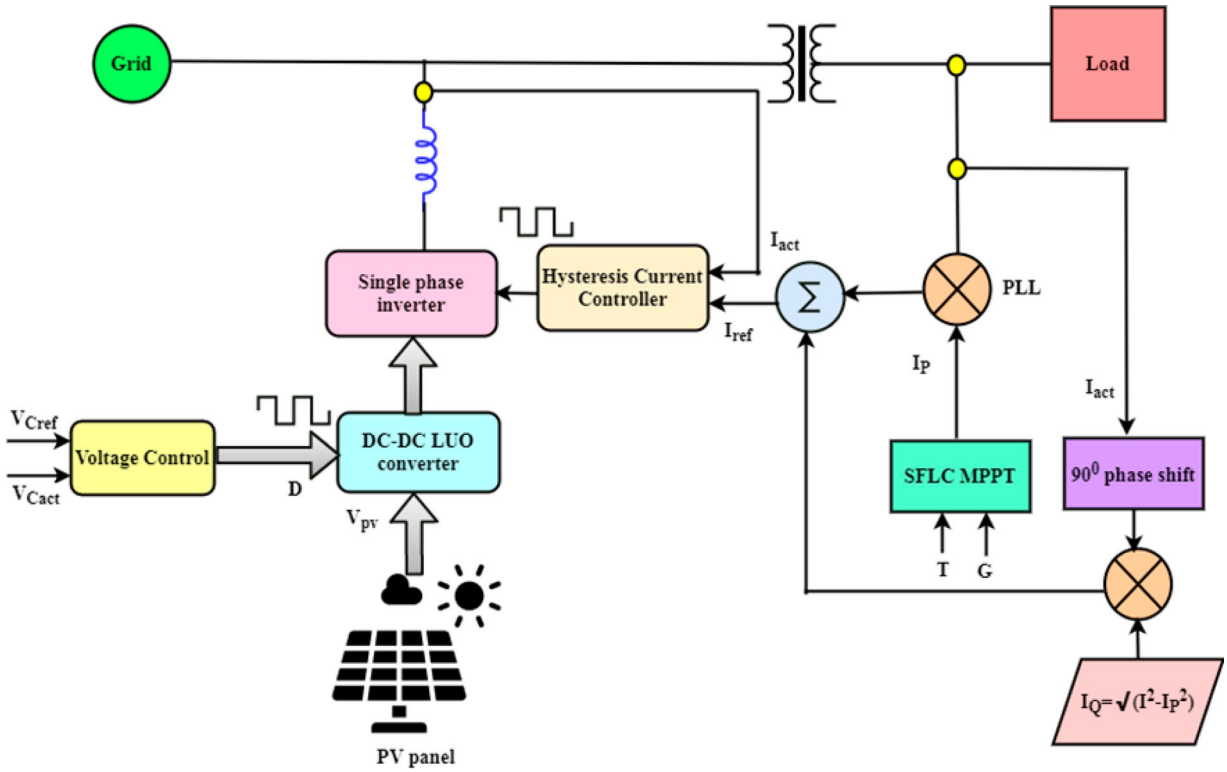

Figure 1. Proposed reactive power compensation system.

Table 1. The impact of different inverter side current controller-based RPC in grid system.

Ref. No	MPPT control strategy	Converter topology	Inverter topology	PF	Transformer requirements	Control topology	Methodology	Benefits
[30]	SSSP with CCM	Buck–Boost converter	1-ϕ single stage	Unity	No	Inverter side current control	Single-stage single-phase grid-connected system(SSSP) achieved through CCM	Low cost, high efficiency
[31]	NA	No	1-ϕ two-level Inverter	NA	No	Inverter side current control	Proportional and resonant control-based current control	Reduce harmonic distortion at low switching frequency
[32]	*P* & O	Boost converter	1-ϕ two-stage Inverter	NA	No	Inverter side current control	F-PI, F-SMC based DC voltage control, PR with RHC as a current control with STGT inverter	Fast and effective method, robustness, oscillation is less
[33]	P & O	Boost converter	1-ϕ Inverter	Unity	Yes	Inverter current control	DCC-based inverter control with SPWM	Control technique is simple; equipment cost is low; high accuracy and reliability
[34]	DC–DC boost converter track MPPT	Boost converter	1-ϕ Inverter	Unity	No	Inverter current control	The reference signal is sensed directly from the grid using HCC	High efficiency, low cost, low THD, robust current regulation
[35]	NA	NA	3-ϕ Inverter	NA	Yes	Inverter side current control	Grid-interfaced three-phase inverter is controlled by adaptive network-based fuzzy inference control	Steady-state fluctuations decreased, robustness, even parametric uncertainties ANFIS enhance the power quality
[36]	P & O	SEPIC converter	3-ϕ Inverter	Unity	No	Inverter current control	Reactive power compensation is achieved through UPFC	Simple control system, high dynamic response
[37]	ANN	Buck–Boost converter	1-ϕ Inverter	NA	Yes	Inverter side current control	ADP-ANN is used for optimal control	Ensuring the overall performance, reliability and controllability
[38]	P & O	Buck–Boost converter	1-ϕ Inverter	Unity	Yes	Inverter side current control	1-ϕ DTDPLL is used in current and voltage control for both grid-connected isolated mode.	Simple, step size is reduced, transient response is fast and smooth
Proposed work	SFLC	LUO	1-ϕ Inverter	Unity	Yes	Inverter side current control	The hysteresis current controller and Self-Tuned MPPT Fuzzy Controller have been integrated for RPC	Control technique is simple, low THD, low cost, ensuring the overall performance, reliability and controllability

Generally, there are different RPC techniques are available for the grid-connected PV systems; amongst other techniques, the inverter side current controller-based RPC plays a vital role. Table 1 shows the impact of different inverter side current controllers-based reactive power compensation in grid systems, in which various MPPT control strategies, converter topologies and inverter control strategies have been involved with the benefits. Based on the benefits of grid-connected PV system, the self-tuned fuzzy inverter control is developed with LUO converter for RPC.

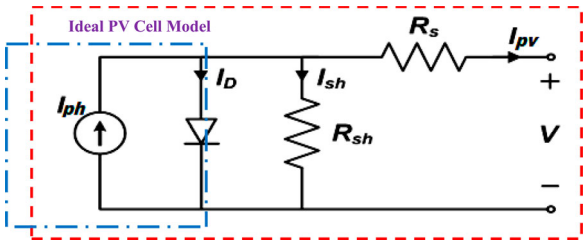

Figure 2. DC equivalent circuit of single-diode model of PV cell.

2.1. Modelling of PV panel

The DC equivalent circuit of the single-diode representation of PV panel is shown in Figure 2. It consists of the current source, diode, series and parallel resistors. The mathematical modelling of PV panel is given below [39,40].

Let, I_{pv} be the photovoltaic current produced by the solar cell, which is determined as follows:

$$I_{pv} = I_{ph} - I_D - I_{sh} \tag{2}$$

Here, the I_{ph} can vary with respect to the temperature and irradiation values, which are illustrated as follows:

$$I_{ph} = \frac{G}{Gref}(I_{sc,ref} + \mu_{sc}.\Delta T) \tag{3}$$

Consequently, the reverse saturation current I_0 can vary based on the temperature of the cell specified by the schottky diode equation, in which the diode current is computed as follows:

$$I_D = I_0\left(\exp\left(\frac{V + IRs}{a}\right)\right) \tag{4}$$

Similarly, the solar cell shunt current is computed by using the cell series resistance value, which is shown below:

$$I_{sh} = \frac{V + IR_s}{R_p} \tag{5}$$

At last, the final solar PV current is given below

$$I_{pv} = \frac{G}{Gref}(I_{sc,ref} + \mu_{sc}.\Delta T) - I_0\left(\exp\left(\frac{V + IRs}{a}\right)\right) - \frac{V + IR_s}{R_p} \tag{6}$$

Moreover, the output of PV panel load current and voltage are determined based on the dynamic performance calculations.

2.2. Self-Tuned Fuzzy Logic Controller-based MPPT

Initially, the maximum power from the solar PV systems is extracted by using the Self-Tuned Fuzzy Logic Controller Integrated Maximum Power Point Tracking (SFLC-MPPT) controller. Here, this technique is mainly implemented to obtain the best output results under varying irradiance and temperature conditions. The main reason for deploying SFLC is to reduce the complexity of controlling methodology and to increase the performance of static and dynamic power systems. The major stages involved in this controlling algorithm are fuzzification, rules generation and defuzzification. In this model, the irradiance and temperature values are taken as the inputs and reference current is produced as the output of the system. It is the maximum current generated from the solar system and is supplied to the grid with the unity power factor. Typically, the climatic conditions can vary in India, where the minimum temperature is 15°C in winter and 45°C in summer. Similarly, the irradiance can vary from 100 to 1000 Watt/m^2, where the nominal value is assumed as 400 to 700 Watt/m^2.

Table 2. Fuzzy rules set.

	T						
G	VVL	VL	L	M	H	VH	VVH
VVL	VL	VL	VL	VL	VL	VL	VL
VL	VL,L	VL,L	VL,L	VL,L	VL,L	VL,L	VL,L
L	L,M	L,M	L,M	L,M	L,M	L,M	L,M
M	M,L	M,L	M,L	M,L	M,L	M,L	M,L
H	M,H	M,H	M,H	M,H	M,H	M,H	M,H
VH	H,M	H,M	H,M	H,M	H,M	H,M	H,M
VVH	H,VH	H,VH	H,VH	H,VH	H,VH	H,VH	H,VH

In the proposed FLC model, the input temperature and irradiance measures are split into seven fuzzy subsets and 91 rules have been generated for attaining an accurate maximum power point. The established fuzzy rules are depicted in Table 2, C. R. Algarín et.al. [41] (2017) have selected the following linguistic variables: Very Very Low (VVL), Very Low (VL), Low (L), Medium (M), High (H), Very High (VH) and Very Very High (VVH).

Fuzzy rules
1. When (temperature becomes VVL) and (irradiation becomes VVL) then (I_s* becomes VL).
2. When (temperature becomes L) and (irradiation becomes M) then (I_s* becomes M).
3. When (temperature becomes M) and (irradiation becomes H) then (I_s* becomes L).
4. When (temperature becomes H) and (irradiation becomes VH) then (I_s* becomes H).
5. When (temperature becomes VH) and (irradiation becomes VL) then (I_s* becomes VH).

The mentioned fuzzy rules have been used in the PV system for optimally tracking the power points. Figure 3 shows the generated membership functions of the SFLC controller, where Figure 3(a) represents the input temperature, Figure 3(b) represents the input irradiance and Figure 3(c) represents the output of the SFLC reference current. Moreover, the relative difference between the input and output reference current is illustrated for irradiance and temperature measures in Figure 4.

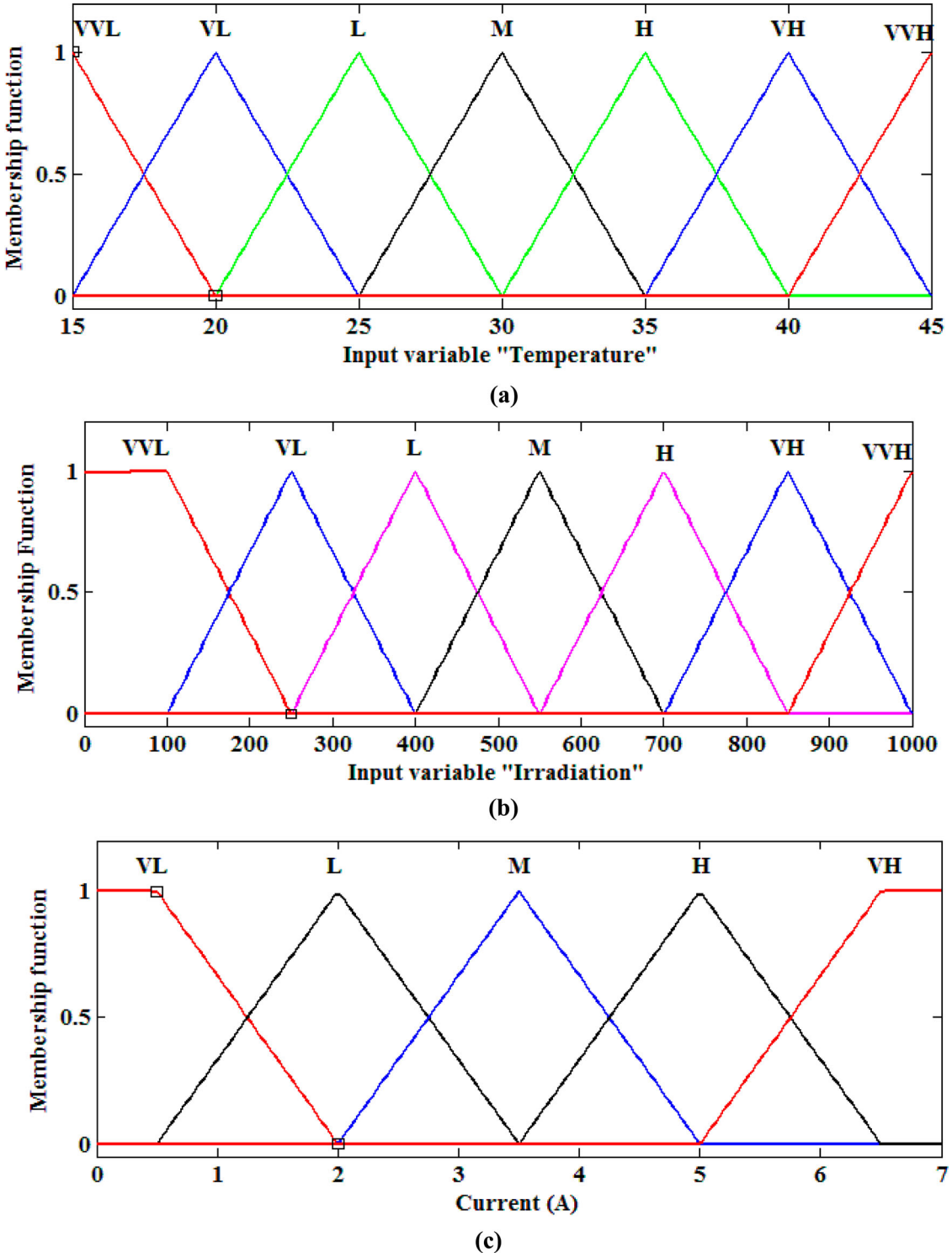

Figure 3. Fuzzy membership functions: (a) input temperature, (b) input irradiation and (c) output SFLC reference current.

3. Analysis of LUO converter

In order to maintain a constant output voltage (V_0) from a variable input voltage (V_{in}) from PV panel and reduce a ripple content, the DC–DC LUO converter is utilized in the proposed system design. The LUO converter is one of the most suitable techniques for solar PV systems when compared to the other existing approaches. The PV array's voltage can vary with respect to the load. Then, the circuit representation of this converter is shown in Figure 5(a). According to the current passing through the inductor (L_1), the converter topology can operate in continuous conduction mode (CCM) and discontinuous conduction mode (DCM). The output voltage of the LUO converter (V_0) is stated by,

$$V_0 = \frac{\alpha}{1-\alpha} V_{in} \tag{7}$$

where "α" indicates the duty cycle of switch S.

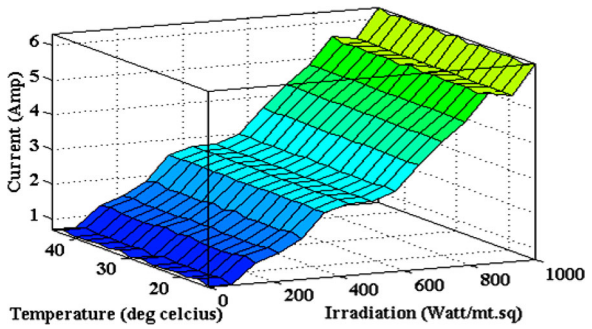

Figure 4. Relative differentiation between the inputs and output of SFLC module.

3.1. LUO converter: modes of operation

The operating principles of the LUO converter are analysed based on two operating modes (ON condition and OFF condition) of the switch [42,43].

Mode1: The turn ON period of LUO converter circuit diagram is shown in Figure 5(b). When the switch is in the ON position, the input current could be $i_{in} = i_{L2} + i_{L1}$. Here, the supply voltage is triggered by inductor L_1, during this time; the i_{L2} draws power by using the capacitor C_1 and source. Then, it helps to increase the current of i_{L1} and i_{L2}, where L is the inductor of the converter.

Mode 2: The turn OFF period of LUO converter circuit diagram is shown in Figure 5(c). Until the switch is off, the energy consumed through the supply remains zero and, i_{L1} goes through the diode to recharge the C_1. Meanwhile, i_{L2} current diffuses along the (R&C_2) connection. Both i_{L1} and i_{L2} inductor current starts to decrease. There is a slight difference in the inductor current i_{L2} and i_{L1}, hence, consider $i_{L2} \approx I_{L2}$ and $i_{L1} \approx I_{L1}$. Where, I_{L2} and I_{L1} are the mean values of the inductor current L_2 and L_1. When the switch is in off state, the charge on capacitor C_1 increases, as shown in Equation (8)

$$Q_{-} = (1 - \propto) I_{L_2} \tag{8}$$

During the switch-on period, it decreases

$$Q_{-} = \propto I_{L_2}, \tag{9}$$

where $\propto = \frac{T_{on}}{T}$.

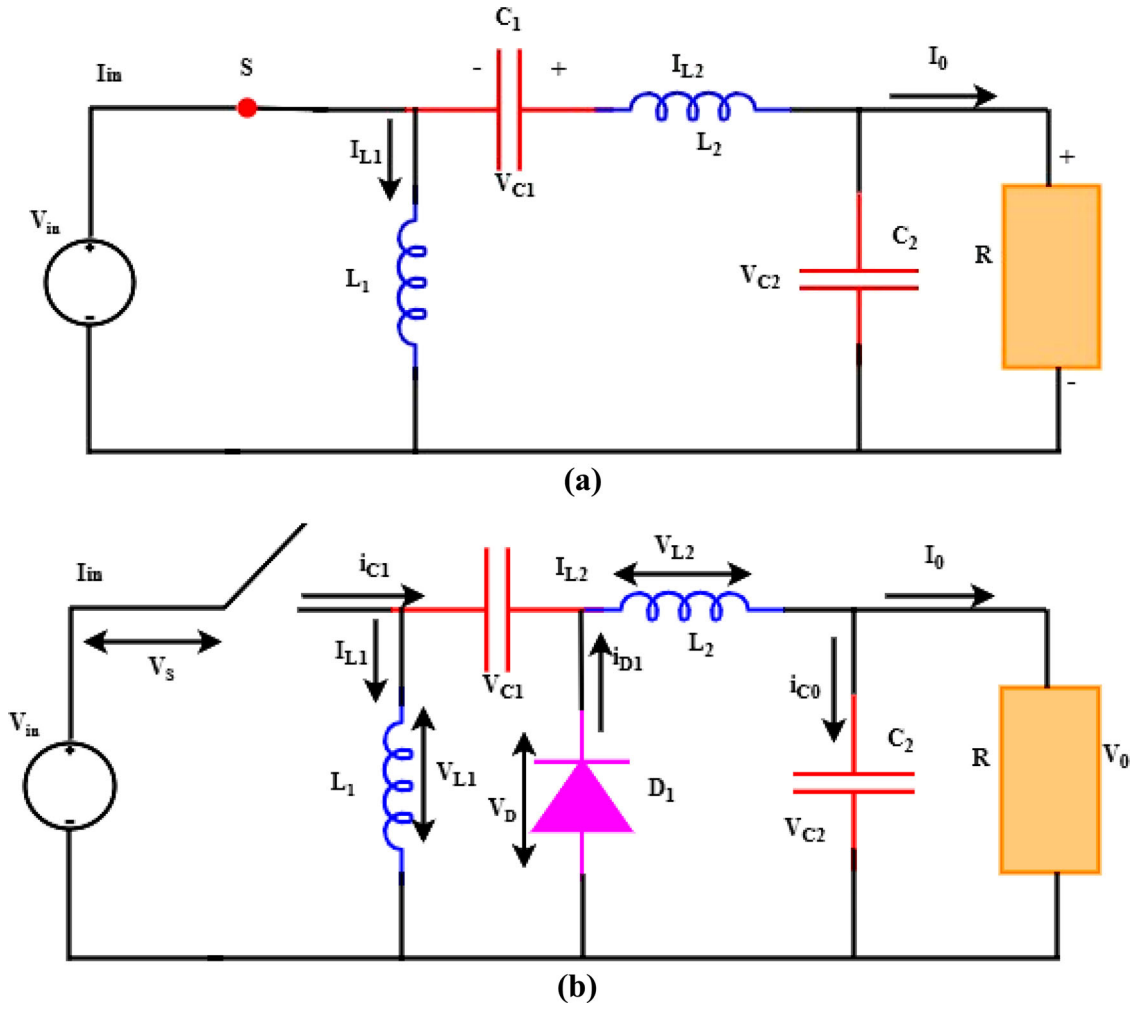

Figure 5. (a) LUO converter circuit diagram, (b) during switch-ON period, (c) during switch-OFF period and (d) voltage and current waveforms of LUO converter. Where S – Switch; D – Diode; C – Capacitor; V_{in} – Input Voltage; V_0 – Output Voltage; I_{in} – Input Current; I_0 – Output Current.

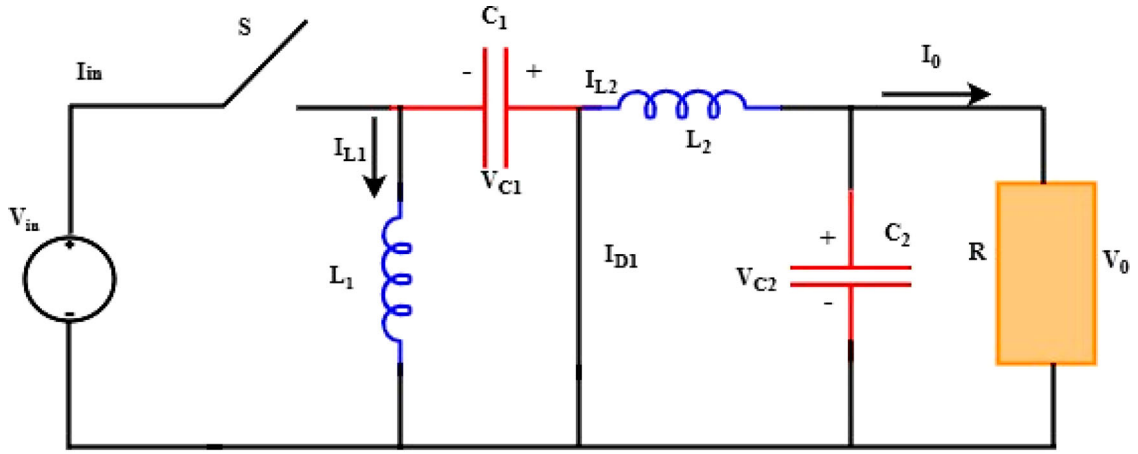

(c)

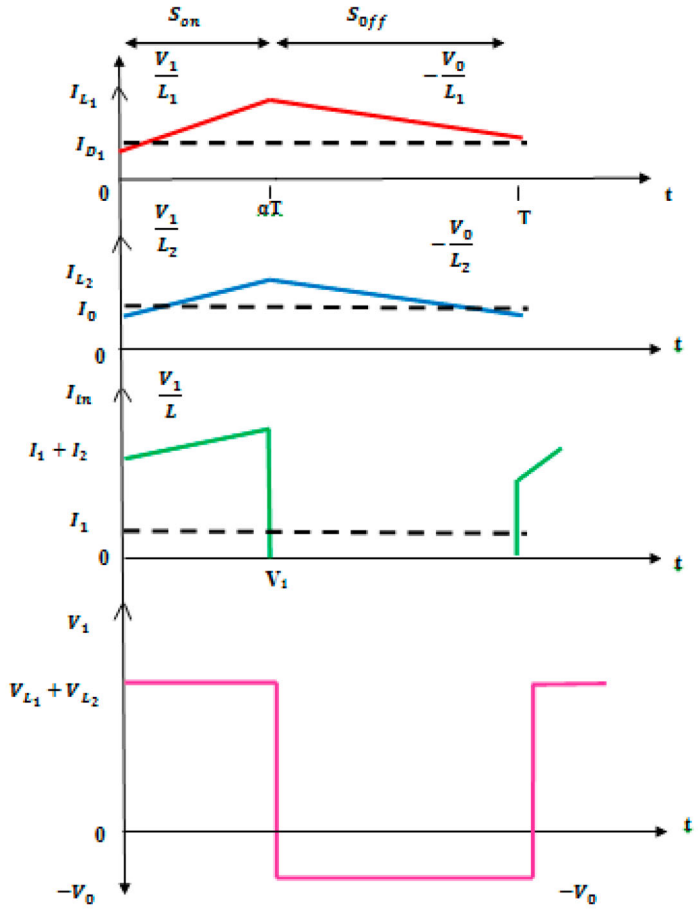

(d)

Figure 5. Continued.

The inductor current I_{L2} in Equation (10) is obtained from the period, $Q_- = Q_+$ using the relation,

$$I_{L_2} = \frac{1-\propto}{\propto} I_{L_1} \tag{10}$$

Even if the C_2 capacitor serves here as LPF, the expression of the I_0 is shown in Equation (11)

$$I_{L_2} = I_0 \tag{11}$$

The source current $i_{L1} + i_{L2} = i_{in} = i_S$ for the switch-on time period and $i_{in} = 0$ when it's switch-off. Equation (12) thus represents the source average current, I_{in}.

$$\begin{aligned} I_{in} &= \propto * i_{D_1} = \propto (i_{L_1} + i_{L_2}) \\ &= \propto \left(1 + \frac{1-\propto}{\propto}\right) I_{L_1} = I_{L_1} \end{aligned} \tag{12}$$

Table 3. The instantaneous values of the current and voltage during ON/OFF condition of the switch.

$V_S = \begin{cases} 0, & for\ 0 < t \le dT \\ V_0 + V_{in}, & for\ dT < t \le T \end{cases}$	$i_1 = i_S = \begin{cases} i_{L_1}(0) + i_{L_2}(0) + \frac{V_{in}}{L_1}t, & for\ 0 < t \le dT \\ 0 & for\ 0 < t \le dT \end{cases}$
$V_D = \begin{cases} V_0 + V_{in}, & for\ 0 < t \le dT \\ 0 & for\ dT < t \le T \end{cases}$	$i_C \approx \begin{cases} i_{L_2}(0) + \frac{V_{in}}{L_{12}}t & for\ 0 < t \le dT \\ -i_{L_1}(dT) + \frac{V_0}{L_1}(t - dT) - I_0, & for\ 0 < t \le dT \end{cases}$
$V_{L_1} = \begin{cases} V_{in}, & for\ 0 < t \le dT \\ -V_0 & for\ dT < t \le dT \end{cases}$	$i_{L_1} = \begin{cases} i_{L_1}(0) + \frac{V_{in}}{L_1}t, & for\ 0 < t \le dT \\ i_{L_2}(dT) - \frac{V_0}{L_1}(t - dT), & for\ 0 < t \le dT \end{cases}$
$V_{L_2} = \begin{cases} V_{in}, & for\ 0 < t \le dT \\ -V_0, & for\ dT < t \le T \end{cases}$	$i_{L_2} = \begin{cases} i_{L_2}(0) + \frac{V_{in}}{L_2}t, & for\ 0 < t \le dT \\ i_{L_2}(dT) - \frac{V_0}{L_2}(t - dT), & for\ 0 < t \le dT \end{cases}$

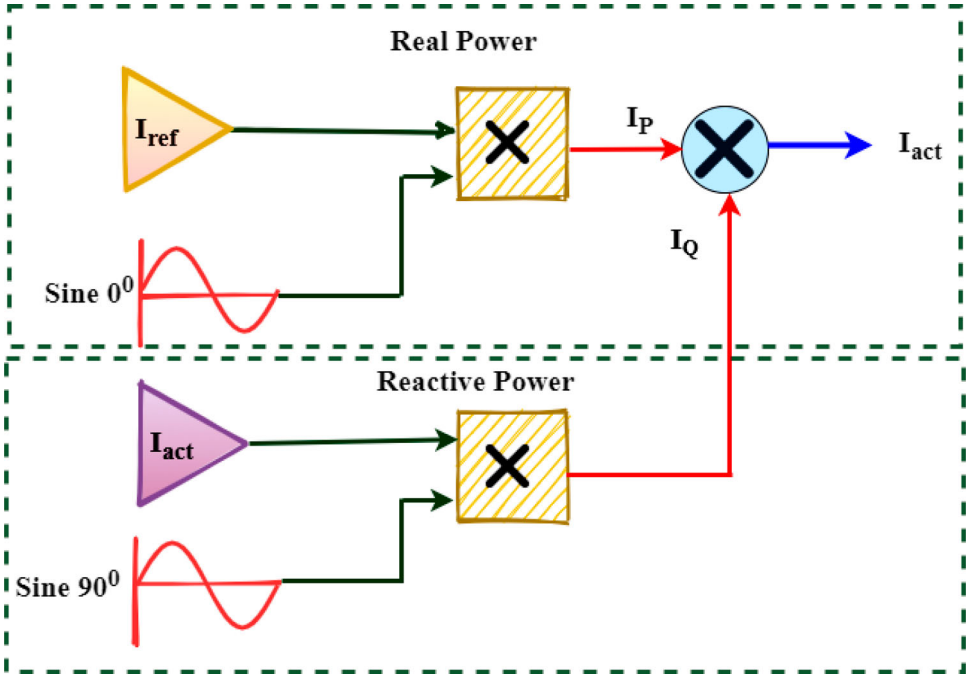

Figure 6. Real and reactive power compensation.

From Equation (13), the output current is

$$I_0 = \frac{1 - \propto}{\propto} I_{in} \tag{13}$$

Table 3 shows the instantaneous evaluations of both current and voltage equations. The instantaneous value of the LUO inverter circuit, including its current and the voltage waveform, is shown in Figure 5(d).

4. Reactive power detection and compensation

The single-phase inverter design is an essential component in the proposed system design. Then, the performance of the converter system highly depends on the quality of the inverter reference current control. The aim of implementing the inverter in an integrated grid circuit is to obtain an alternating output current with the reference current. The inverter circuit also provides the reactive power; the schematic representations of real and reactive power compensation and the inverter circuitry are depicted in Figures 6 and 7.

4.1. Shunt Active Power Filters (SAPF)

The Shunt Active Power Filters (SAPF) is one of the most extensively used filtering techniques in industrial sectors, which is mainly used for solving the power quality issues related to reactive power support, load imbalance reduction and current harmonics elimination. Typically, it is connected with the harmonic polluted power system with the help of Point of Common Coupling (PCC). In this work, the functionalities of SAPF have been incorporated with the solar PV systems, where the PV arrays can supply the real power to the load unit. Moreover, it could support both the reactive power supply and eliminating the harmonic simultaneously. Also, it comprises more features like a less environmental burden due to modularity, easily expandable and applicable everywhere.

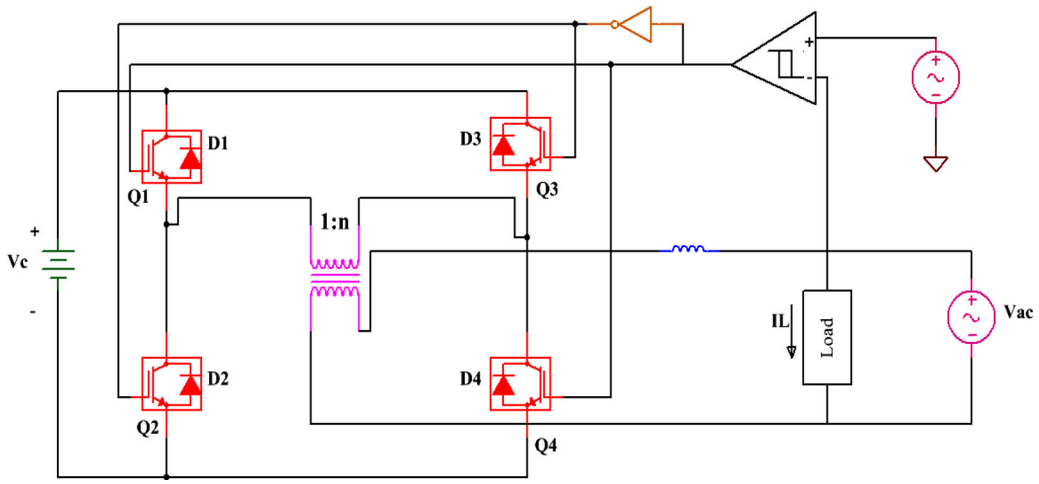

Figure 7. Schematic diagram of inverter circuit.

4.2. Hysteresis current controller

Typically, many issues could arise at the time of connecting solar PV with the grid, in which the power quality is one of the most important factors. Moreover, high PV injection can create some unwanted technical problems on the distribution networks, which lead to power quality issues. In general, different types of filtering techniques are available for reducing the harmonic contents, but it limits the problems like circuit designing complexity, reduced bandwidth, high cost and sensitivity. Thus, an advanced controlling strategy has been developed for controlling the level of THD. Due to this reason, the hysteresis current controller is utilized in the proposed system design to efficiently reduce THD level of the system under IEEE 519_1992 regulations. Also, this work incorporates the features of both hysteresis current controller and SFLC techniques for obtaining better power quality results. In the proposed work, the THD level is reduced without filtering process ∼2%–6% under different irradiation and temperature conditions and also THD level is reduced with filtering technique to 1.87% that meets the regulations of IEEE 519_1992 standard.

5. Results and discussion

In this section, both the simulation and hardware results of the proposed controlling method are analysed for validating the performance outcomes. Here, the MATLAB simulation tool is used to take the analytical results from the PV array. The solar PV panel specifications used in this analysis are presented in Table 4.

5.1. IV and PV characteristics of PV panel

Figures 8 and 9 show the current-voltage (IV) and power voltage (PV) characteristics of the PV panel under varying irradiance and temperature levels. Generally, the IV characteristics are mainly analysed and monitored to estimate the actual power produced by the PV modules concerning the accurate operating conditions. Based on these characteristics, the performance of maximum power extraction by the controlling technique can be estimated. The evaluation shows that the proposed controller design provides a fast and dynamic response with the exact emulation of IV and PV characteristics.

Table 4. Solar PV panel specifications.

Parameters	Specification
Solar panel	100 W
Open circuit voltage V_{OC}	21.6 V
Short circuit current I_{SC}	5.8 A
Maximum voltage V_{MPP}	18.5 V
Maximum current I_{MPP}	5.5 A
Series resistance R_S	0.45 Ω
Parallel resistance R_P	310 Ω

The performance analysis of existing and proposed controller techniques concerning the parameters of input voltage, output voltage, output current and output power at different irradiation and temperature conditions. Table 5 shows the comparisons of different controllers for MPP tracking method at Standard Test Condition (STC) such as temperature is 25°C, irradiation 1000 Watt/m^2. Figure 10 shows that the proposed SFLC-MPPT provides better output voltage, current and power values compared to the traditional controller techniques.

5.2. LUO converter response

Figure 11 shows the LUO converter output voltage and current waveform of 900 Watt/m^2 with 25°C temperature values. This analysis indicates that the ripple voltage and current are constant for different irradiation and temperature conditions.

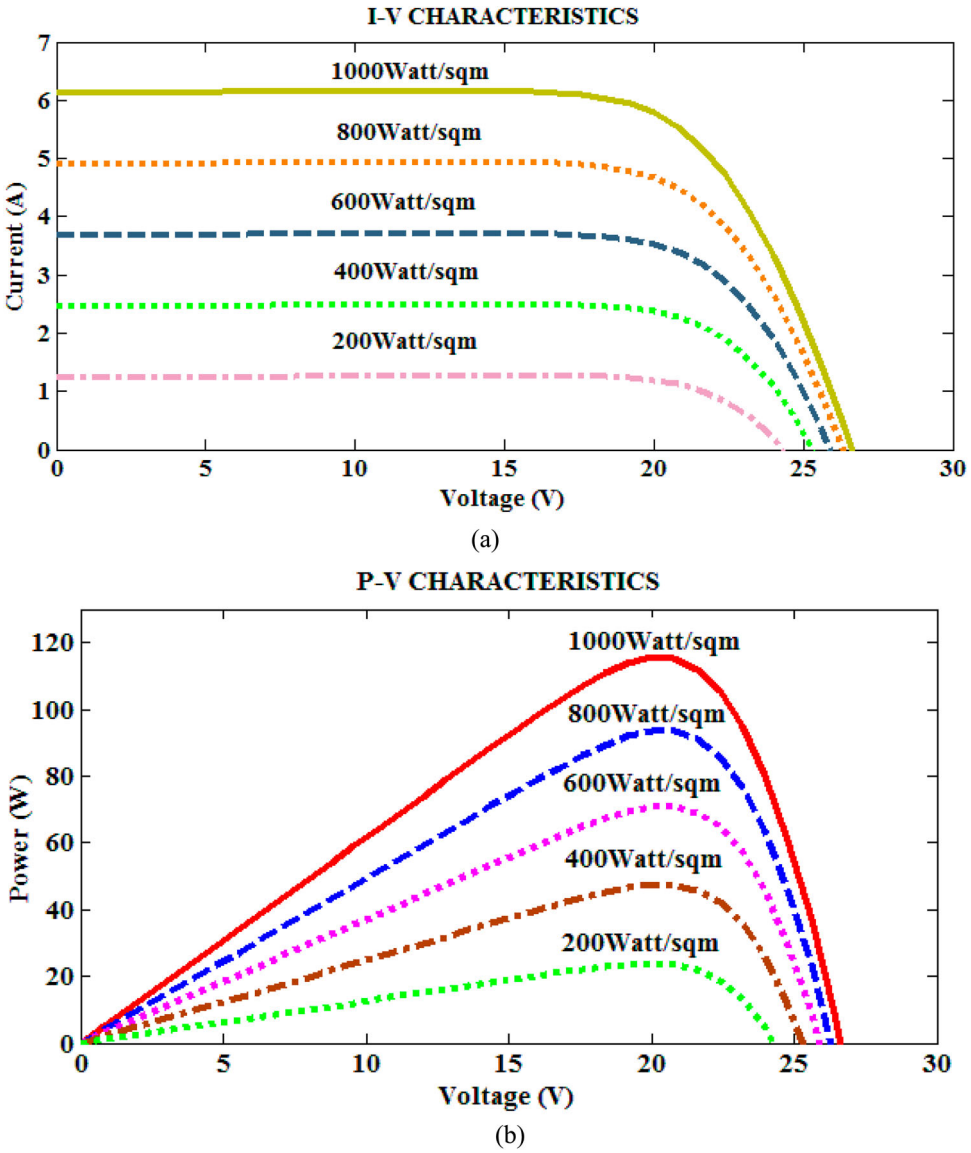

Figure 8. (a) IV and (b) PV characteristics with respect to various irradiance levels.

5.3. Real and reactive power compensation

5.3.1. Injected current variation at different irradiation level

Figure 12(a,b) shows the load, source and injected currents at irradiation levels of 400 and 900 Watt/m^2, 25°C, respectively. It is observed that load current (I_L) 2.26 A is larger than the source current (I_S) 1.9 A for both low and high irradiation levels because the current is injected from the solar panel. At a 400-Watt/m^2 irradiation condition, the inverter of PV system injected reactive current (I_{inj}) component of load current is 0.42 A and at the same time of 900 Watt/m^2 irradiation level load current is 0.38 A. From the graph, it is inferred that the phase angle between the injected current and grid voltage of the system is less which leads to a unity power factor.

5.3.2. Real and reactive power variation at different irradiation level

Figure 13(a,b) analyses the proposed system's real and reactive power supply for 400 and 900 Watt/m^2 irradiation with 25°C temperature values. The evaluation shows that the real power supply to the grid system is 368 W for the irradiance of 400 Watt/m^2 and 328 W for the irradiance of 900 Watt/m^2. Similarly, the reactive power supply to the grid system is 232 VAr for 400 Watt/m^2 and 288 VAr for 900 Watt/m^2. These results depicted an increased amount of reactive power supplied to the grid under high irradiance and constant temperature level. The efficiency of the converter and controller topologies is analysed based on the amount of real and reactive power supplied to the grid system.

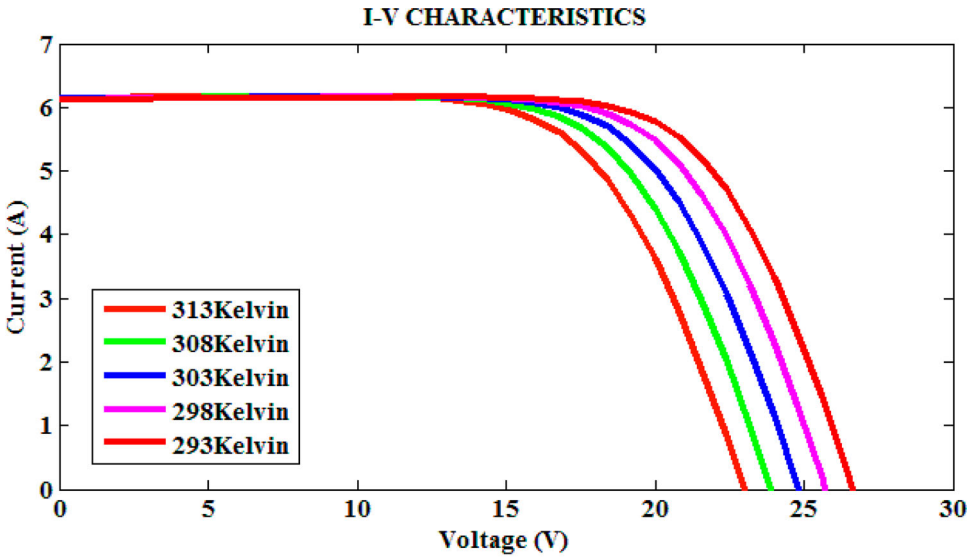

(a)

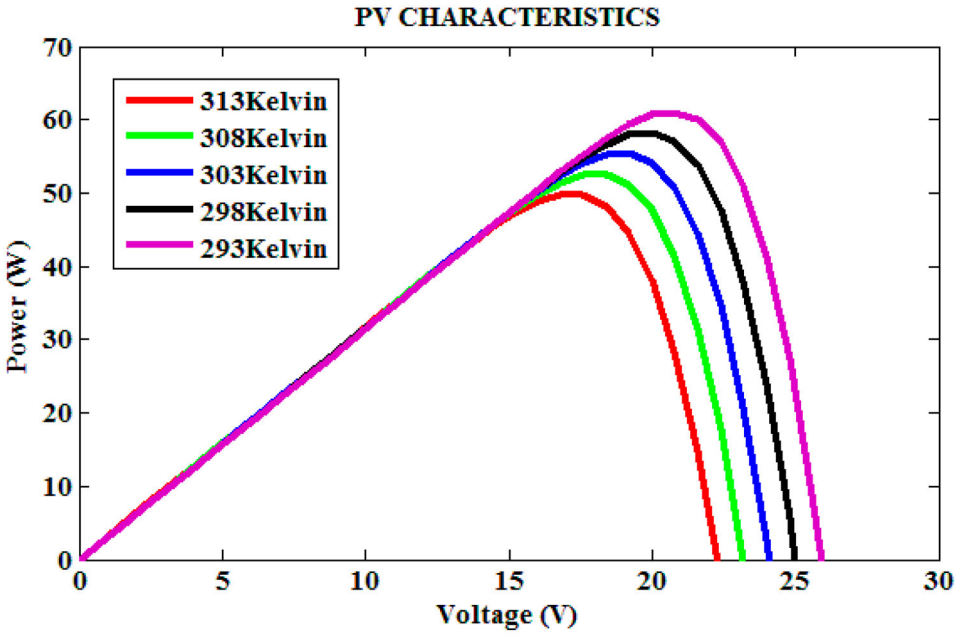

(b)

Figure 9. (a) IV and (b) PV characteristics with respect to varying temperature levels.

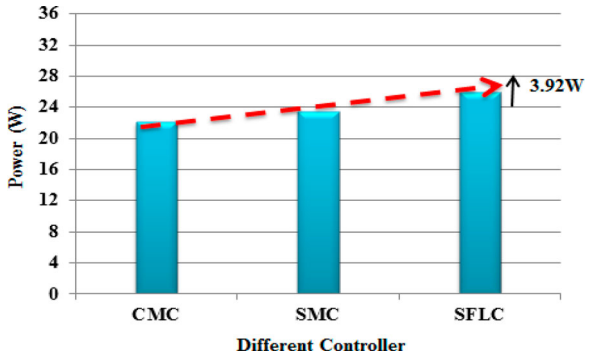

Figure 10. Comparison between existing and proposed controlling techniques.

Table 5. Comparisons of different controllers for MPP tracking at STC.

Parameters	V_{in} (V)	V_{out} (V)	I_{out} (A)	P_{out} (W)
CMC	12	34.5	0.64	22.08
SMC	12	35	0.67	23.45
SFLC	12	36	0.72	26

5.3.3. Injected real and reactive power

Figure 14(a,b) depicts the injected real and reactive power supply to the grid system under varying irradiance of 400 and 900 Watt/m^2 with constant temperature 25°C values. Based on this analysis, it

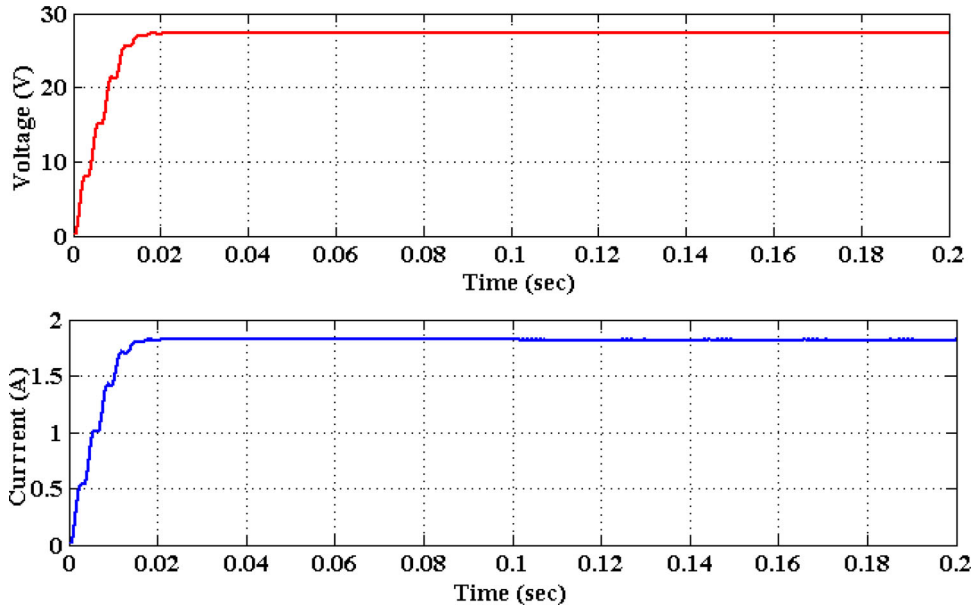

Figure 11. LUO converter output voltage and current.

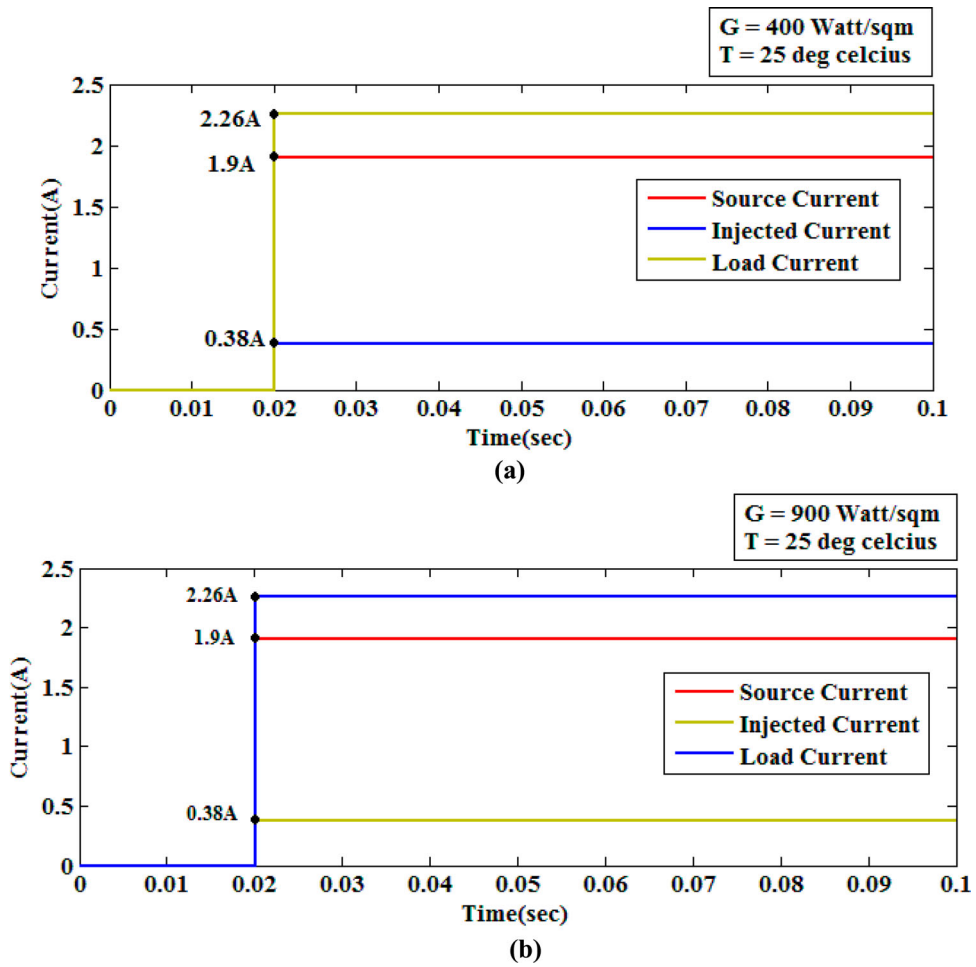

Figure 12. (a) Load, source and injected currents at 400 Watt/m^2 irradiation, 25°C. (b) Load, source and injected currents at 900 Watt/m^2 irradiation, 25°C.

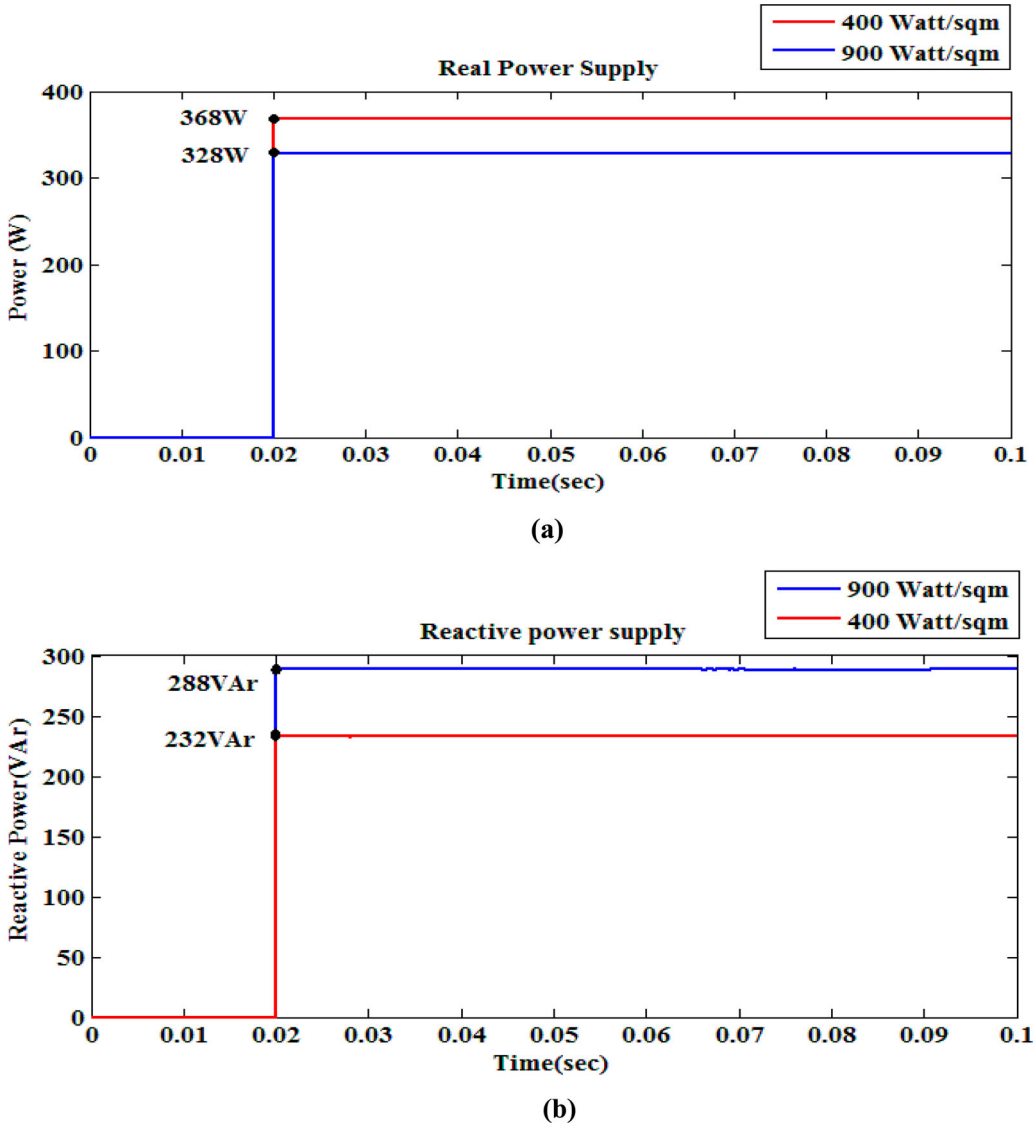

Figure 13. (a) Real power supply – irradiation is 400 and 900 Watt/m^2 at constant temperature 25°C. (b) Reactive power supply – irradiation is 400 and 900 Watt/m^2 at constant temperature 25°C.

is observed that more real power, that is, 80 W, is injected from the source under a high level of irradiance 900 Watt/m^2. Similarly, more reactive power is injected, that is, 88 W for compensation under low irradiance 400 Watt/m^2. Thus, the controller's performance is validated by injecting the real and reactive power from the source.

5.4. Grid voltage and actual current

Figure 15(a,b) shows the grid voltage analysis waveform under varying irradiance, that is, 400 and 900 Watt/m^2, and constant temperature 25°C. The actual current analysis is performed under varying irradiance 400 and 900 Watt/m^2 and constant temperature measures as shown in Figure 16(a,b). This analysis stated that no reactive power has been drawn from the grid systems after compensation under varying irradiance levels.

Table 6 evaluates the simulation parameters of load, source and injected real and reactive power with respect to the irradiance of 400 and 900 Watt/m^2 with temperature 25°C.

5.5. THD analysis

Figure 17 and Table 7 show the total harmonics distortion (THD) analysis of existing and proposed filtering techniques with LCL filter up to harmonics order of 20. The results show that the hysteresis current controller with the Self-Tuned Fuzzy Logic Controller technique reduces the THD value to 1.87% compared to the existing method.

5.6. Comparative analysis

Table 8 compares the actual power (W) of both existing ANFIS-MPPT [44] and proposed SFLC mechanisms with respect to varying irradiance values. From the results, it is shown that the proposed SFLC is more

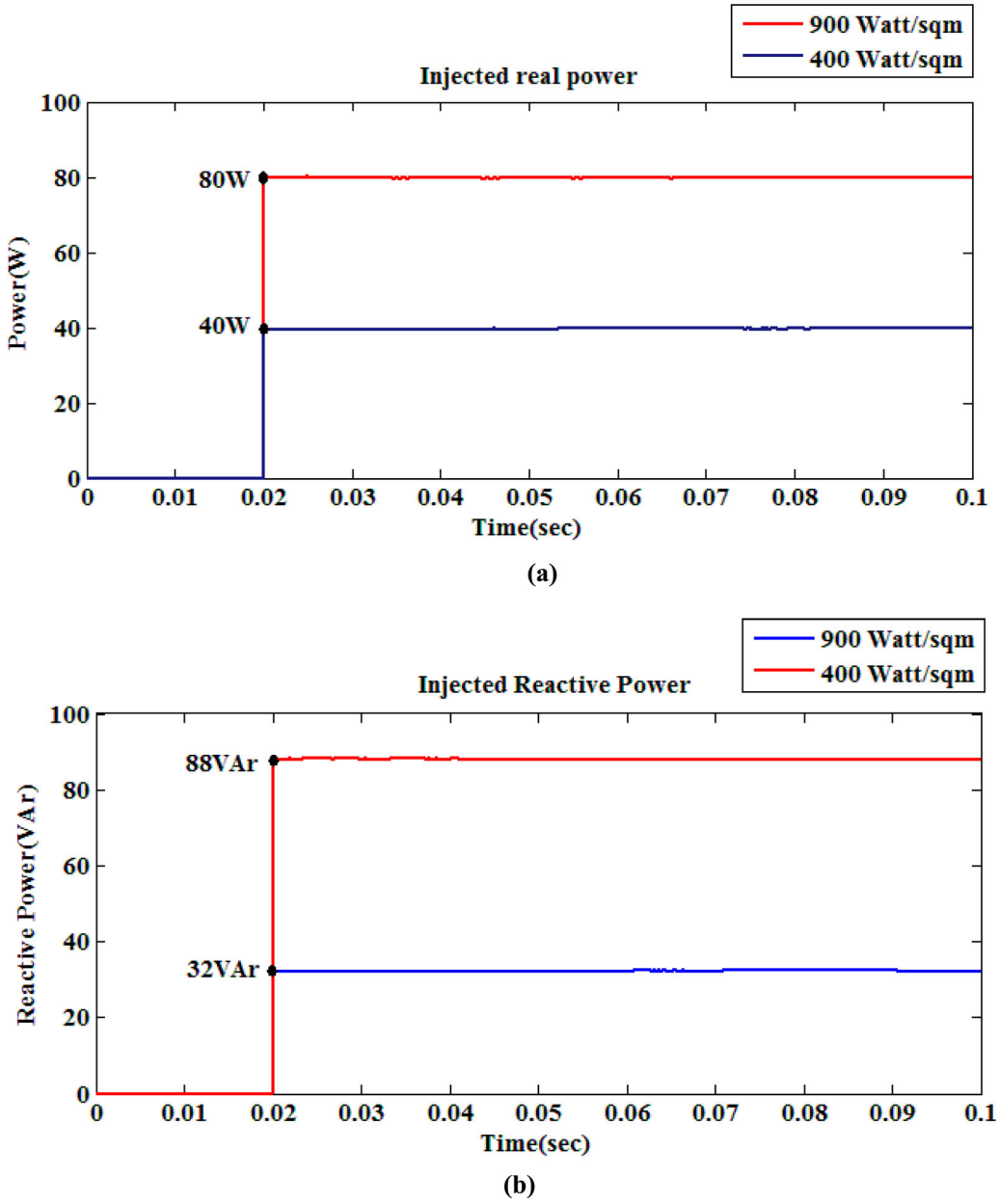

Figure 14. (a) Variation of injected real power at low irradiation (400 Watt/m^2) and high irradiation condition (900 Watt/m^2) at 25°C. (b) Variation of injected reactive power at low irradiation (400 Watt/m^2) and high irradiation condition (900 Watt/m^2) at 25°C.

effective in operating MPP with fast response when compared to the existing technique. Figure 18 shows the tracking capability of solar panel output power for the proposed SFLC-based MPPT scheme.

6. Experimental results

In this work, the experimental setup is performed to validate the proposed work, where the 100 W grid-connected PV system is considered for analysis as shown in Figure 19.

Figure 20(a–c) shows the gate pulse, generated by the PIC microcontroller for inverter, then the grid voltage, current and inverter output voltage of the proposed controller under the irradiance of 900 Watt/m^2 and temperature 25°C values. From the evaluation, it is analysed that the hardware results are precisely close with the MATLAB simulation results. Also, it is evident that the inverter can produce sufficient output current and in phase with respect to the reference current.

Figure 21 shows the comparative analysis of the simulation and hardware results with respect to the real and reactive power injected at varying irradiance levels. This analysis proved that more reactive power is injected at a low irradiance level of 400 Watt/m^2 and more real power is injected at a high irradiance level of 900 Watt/m^2.

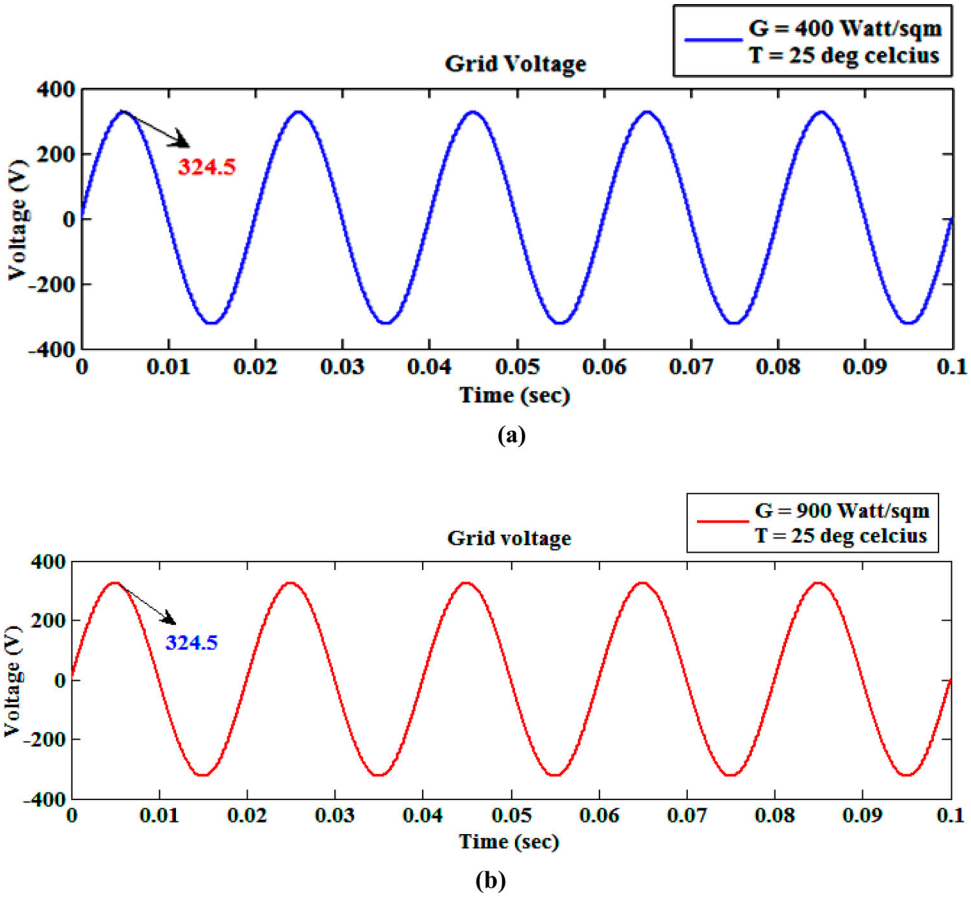

Figure 15. (a) Grid voltage at low irradiation (400 Watt/m^2) and temperature at 25°C. (b) Grid voltage at high irradiation (900 Watt/m^2) and temperature at 25°C.

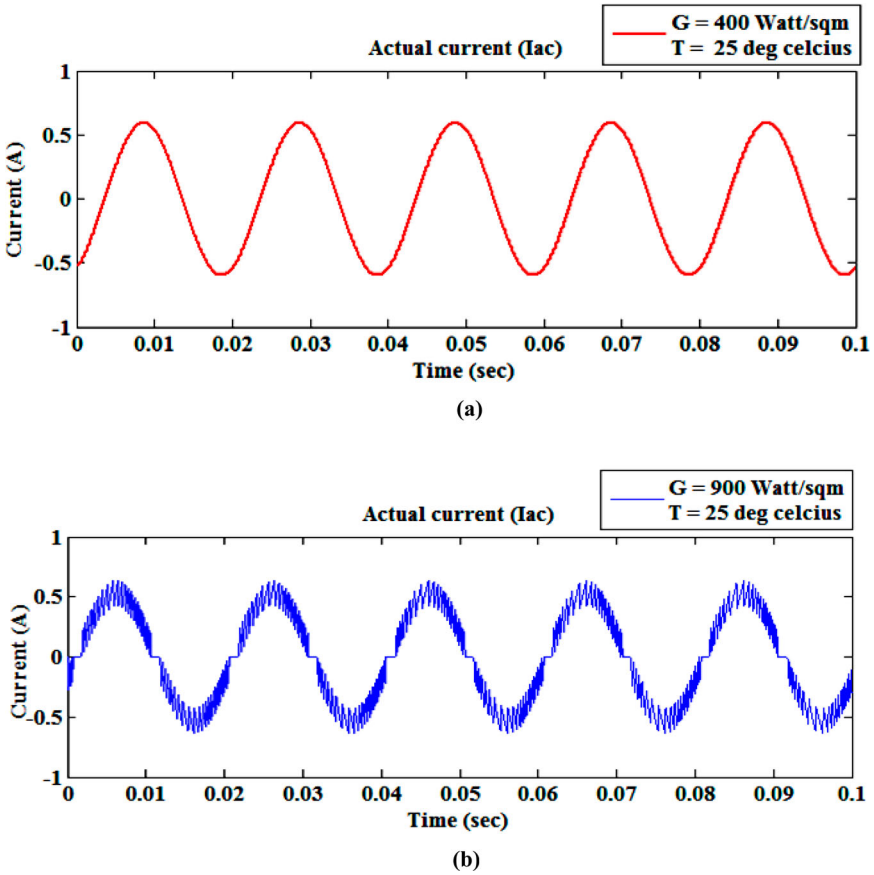

Figure 16. (a) Actual current at low irradiation (400 Watt/m^2) and temperature at 25°C. (b) Actual current at high irradiation (900 Watt/m^2) and temperature at 25°C.

Table 6. Simulation parameters under varying irradiance levels.

Parameters	Irradiation level	
	400 Watt/m^2 and 25°C	900 Watt/m^2 and 25°C
Load resistance R	80 Ω	80 Ω
Load inductance L	200 mH	200 mH
Source voltage	230 V	230 V
Source frequency	50 Hz	50 Hz
Source current	1.9 A	1.9 A
Injected current	0.42 A	0.38 A
Load current	2.26 A	2.26 A
P_L (Load)	408 W	408 W
Q_L	320 VAr	320 VAr
P_s (Source)	368 W	328 W
Q_s	232 VAr	288 VAr
P_i (Injected)	40 W	80 W
Q_i	88 VAr	32 VAr

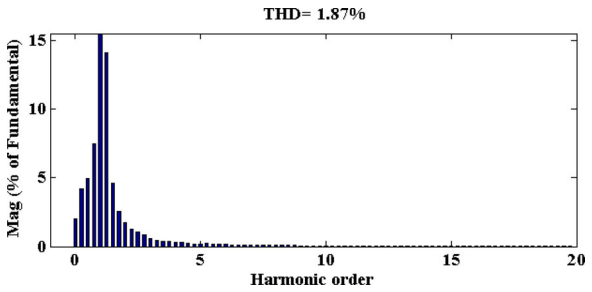

Figure 17. THD analysis of proposed technique up to harmonic order 20.

Table 7. THD analysis between existing and proposed techniques.

Irradiation G, Watt/m^2	$G = 1000$	$G = 800$	$G = 600$	$G = 200$
THD (%) (Existing) (without filter)	22.5	21.2	18.7	18.1
THD (%) (Proposed) (without filter)	16.8	17.6	15.6	16.3
THD (%) (Proposed) (with filter)	1.92	1.87	2.17	1.12

7. Conclusion

In this work, a grid-integrated PV system is designed with SFLC and Hysteresis current controlling topologies

Table 8. Comparison of PV panel output for existing and proposed techniques.

Irradiance (Watt/m^2)	ANFIS-MPPT Actual Power (W)	SFLC-MPPT Actual Power (W)
400	32.6	35.14
600	49.8	52.2
800	72.7	74.04
1000	89.3	91.38

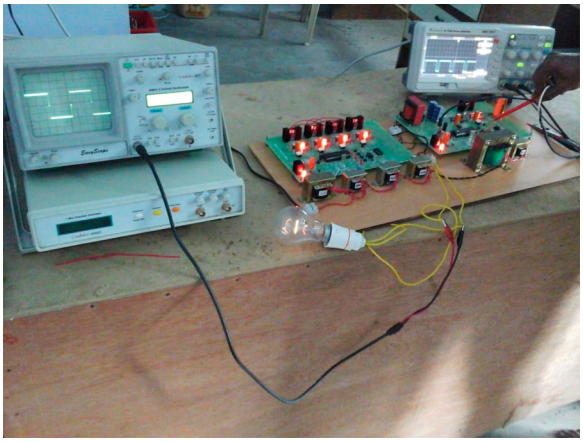

Figure 19. Experimental setup of the proposed grid-connected photovoltaic system (100 W PV panel).

are used in order to achieve efficient reactive power compensation. In this design, a pure sinusoidal grid current is generated with the appropriate phase-shift, which helps to improve the power quality, reactive power compensation and stability under varying irradiation conditions. Also, the sensorless MPPT method is deployed based on the concept of SFLC with reduced cost consumption. The inherent properties of the DC–DC LUO converter used in this work are reduced ripple currents and increased power quality. In this work, both the simulation and experimental studies have been conducted to confirm that the proposed design improves the overall system performance. Moreover, the proposed topology could be

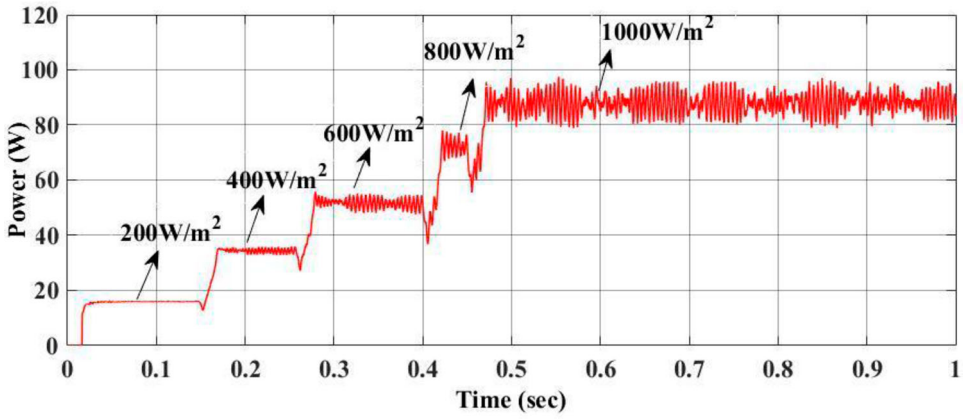

Figure 18. Tracking capability of solar panel output power for the proposed SFLC-based MPPT scheme.

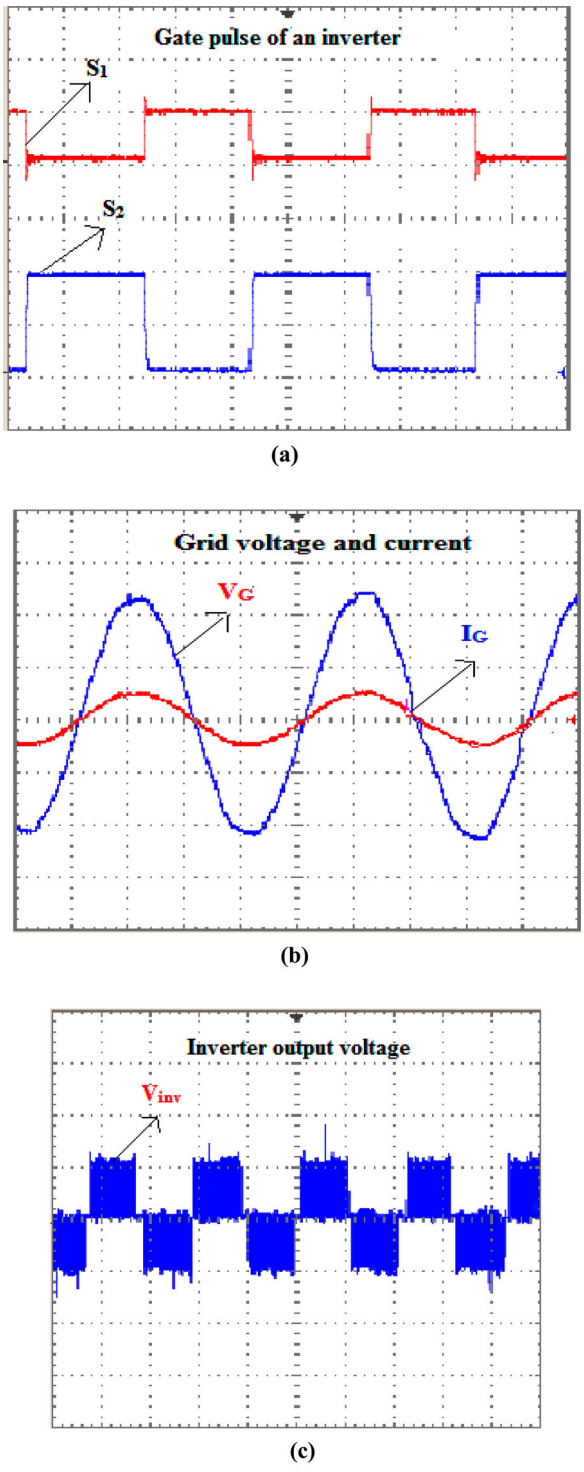

Figure 20. (a) Gate pulse of an inverter. (b) Gate voltage and current. (c) Inverter output voltage.

applied to systems, where substantial reactive power support and simple control circuit is required. However, in the case of systems with varying reactive power requirements, the controlling topology can be modified to ensure that the reactive power is not overcompensated.

In the future, this work can be extended by implementing a new converter and controller topologies for a three-phase grid system.

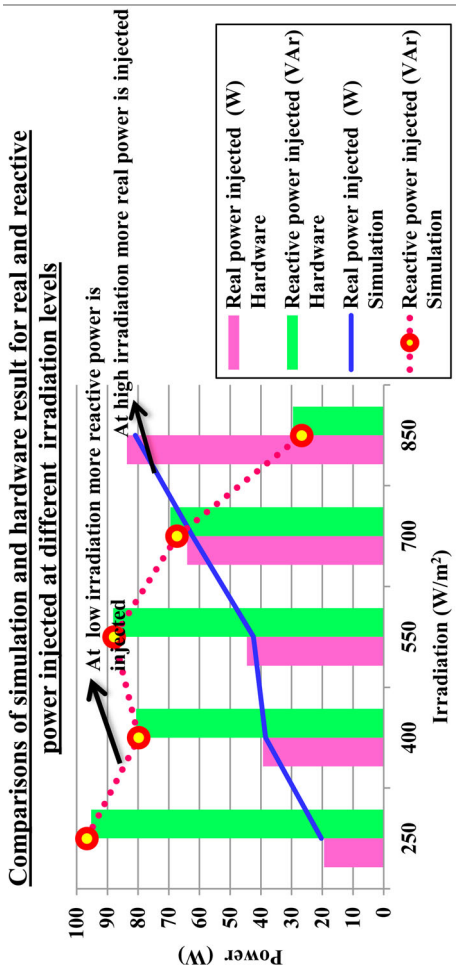

Figure 21. Comparative analysis between the simulation and hardware results.

Acknowledgements

The authors are also thankful to the World Bank sponsored Technical Education Quality Improvement Program (TEQIP) institute of Alagappa Chettiar Government College of Engineering and Technology, Karaikudi, Tamilnadu, India for providing all support to complete this research work.

Disclosure statement

No potential conflict of interest was reported by the author(s).

References

[1] Nwaigwe K, Mutabilwa P, Dintwa E. An overview of solar power (PV systems) integration into electricity grids. Mater Sci Energy Technol. 2019;2(3):629–633.
[2] Podder AK, Roy NK, Pota HR. MPPT methods for solar PV systems: a critical review based on tracking nature. IET Renew Power Gener. 2019;13(10):1615–1632.
[3] Kumar R, Singh S. Solar photovoltaic modeling and simulation: as a renewable energy solution. Energy Rep. 2018;4:701–712.
[4] Abdulrazzaq AA, Ali AH. Efficiency performances of two MPPT algorithms for PV system with different solar panels irradiances. Int J Power Electron Drive Syst (IJPEDS). 2018;9(4):1755–1764.
[5] Krauter S. Simple and effective methods to match photovoltaic power generation to the grid load profile for a PV based energy system. Sol Energy. 2018;159:768–776.
[6] Rallabandi V, Akeyo OM, Jewell N, et al. Incorporating battery energy storage systems into multi-MW grid connected PV systems. IEEE Trans Ind Appl. 2018;55(1):638–647.
[7] Jana J, Samanta H, Bhattacharya KD, et al. Design and development of high efficiency five stage battery charge controller with improved MPPT performance for solar PV systems. Int J Renew Energy Res (IJRER). 2018;8(2):941–953.
[8] Singh O, Gupta SK . A review on recent mppt techniques for photovoltaic system. IEEMA Engineer Infinite Conference at (ETechNxT). New Delhi,India. 2018;1–6.
[9] Abdelwahab SAM, Hamada AM, Abdellatif WS. Comparative analysis of the modified perturb & observe with different MPPT techniques for PV grid connected systems. Int J Renew Energy Res. 2020;10(1):55–164.
[10] Kumar N, Ieee M, Hussain I, et al. Self-adaptive incremental conductance algorithm for swift and ripple free maximum power harvesting from PV array. Trans Ind Inform. 2017;3203:1–10.
[11] Naick BK. Fuzzy logic controller based PV system connected in standalone and grid connected mode of operation with variation of load. Int J Renew Energy Res. 2017;7(1):311–322.
[12] Sun Y, Li S, Lin B, et al. Artificial neural network for control and grid integration of residential solar photovoltaic systems. IEEE Trans Sustain Energy. Oct. 2017;8(4):1484–1495.
[13] Dehghani M, Taghipour M, Gharehpetian GB, et al. Optimized fuzzy controller for MPPT of grid-connected PV systems in rapidly changing atmospheric conditions. J Mod Power Syst Clean Energy. 2020;9(2):376–383.
[14] Chaitanya Pansare SKS. Analysis of a modified positive output Luo converter and its application to solar PV system. IEEE-PSEC;Cincinnati, OH, USA. 2017;1–6.
[15] Zeraati M, Golshan MEH, Guerrero JM. Voltage quality improvement in low voltage distribution networks using reactive power capability of single-phase PV inverters. IEEE Trans Smart Grid. 2018;10(5):5057–5065.
[16] Bajaj M, Rana AS. Harmonics and reactive power compensation of three phase induction motor drive by photovoltaic-based DSTATCOM. Smart Sci. 2018;6(4):319–329.
[17] Arulmurugan R. Photovoltaic powered transormerless hybrid converter with active filter for harmonic and reactive power compensation. ECTI Trans Electr Eng Electron Commun. 2018;16(2):44–51.
[18] Ouai A, Mokrani L, Machmoum M, et al. Control and energy management of a large scale grid-connected PV system for power quality improvement. Sol Energy. 2018;171:893–906.
[19] Smadi AA, Lei H, Johnson BK. Distribution system harmonic mitigation using a PV system with hybrid active filter features. North American Power Symposium (NAPS), IEEE,Wichita, KS, USA. 2019;1–6.
[20] Shah P, Singh B. Low-voltage ride-through operation of grid interfaced solar PV system enabling harmonic compensation capabilities. IET Renew Power Gener. 2019;14(12):2100–2113.
[21] Gayatri M, Parimi AM, Kumar AP. A review of reactive power compensation techniques in microgrids. Renew Sustain Energy Rev. 2018;81:1030–1036.
[22] Zhang J. Unified control of Z-source grid-connected photovoltaic system with reactive power compensation and harmonics restraint: design and application. IET Renew Power Gener. 2017;12(4):422–429.
[23] Ali Z, Christofides N, Hadjidemetriou L, et al. Photovoltaic reactive power compensation scheme: an investigation for the Cyprus distribution grid. IEEE International Energy Conference (ENERGYCON); Limassol, Cyprus. 2018;1–6.
[24] Li H, Wen C, Chao K-H, et al. Research on inverter integrated reactive power control strategy in the grid-connected PV systems. Energies. 2017;10(7):912.
[25] Wang J, Luo F, Ji Z, et al. An improved hybrid modulation method for the single-phase H6 inverter with reactive power compensation. IEEE Trans Power Electron. 2017;33(9):7674–7683.
[26] Pandey SK, Kumar S, Singh B. LCO-FLL control for single-phase utility integrated single-stage solar PV system. IET Renew Power Gener. 2018;12(16):1941–1948.
[27] Bhole N, Bhambhori S. Enhancement of power quality in grid connected photovoltaic system using predictive current control technique. 2017;5:549–553.
[28] Beena V, Jayraju M, Sebin K. Active and reactive power control of single phase transformerless grid connected inverter for distributed generation system. Int J Appl Eng Res. 2018;13:150–157.
[29] Chourasiya S, Agrawal S, Palwalia DK. Performance measure of shunt active power filter applied with intelligent control technique. J Power Technol. 2020;100(3):272–278.
[30] Jain S, Agarwal V. New current control based MPPT technique for single stage grid connected PV systems. Elsevier. 2007;48:625–644.
[31] Escobar JMSG, Lopez-Sanchez MJ. Inverter-side current control of a single-phase inverter grid connected through an LCL filter. IECON 2014 – 40th Annual Conference of the IEEE Industrial Electronics Society; 2014. p. 5552–5558.

[32] Zeb K, Islam SU, Din WU, et al. Design of fuzzy-PI and fuzzy-sliding mode controllers for single-phase two-stages. Electronics. 2019; 8:1–19.
[33] Hassaine L, Bengourina MR. Control technique for single phase inverter photovoltaic system connected to the grid. Energy Rep. 2019; 6:200–2008.
[34] Rahim NA, Selvaraj J. Krismadinata. Hysteresis current control and sensorless MPPT for grid-connected photovoltaic systems. 2007 IEEE International Symposium on Industrial Electronics, Vigo, Spain. 2007; 572–577.
[35] Kakkar S, Ahuja RK, Maity T. Performance enhancement of grid-interfaced inverter using intelligent controller. Meas Control. 2020;53:551–563.
[36] Dash R, Swain SC. Effective power quality improvement using dynamic activate compensation system with renewable grid interfaced sources. Ain Shams Eng. J. 2018;9(4):2897–2905.
[37] Bama S, Punitha K. Artificial neural network for control and grid integration of floating solar. Int J Adv Res Electr Electron Instrum Eng. 2018;7(11):3974–3984.
[38] Panda A, Pathak MK, Srivastava SP. A single phase photovoltaic inverter control for grid connected system. Indian Acad Sci. 2016;41(1):15–30.
[39] Bellia H. A detailed modeling of photovoltaic module using MATLAB. NRIAG J Astron Geophys. 2014;3(1): 53–61.
[40] Venkatesan S, Saravanan M. Simulation and experimental validation of new MPPT algorithm with direct control method for PV application. J Renew Sustain Energy. 2016;8(4):043503.
[41] Algarín CR, Giraldo JT, Álvarez OR. Fuzzy logic based MPPT controller for a PV system. Energies. 2017;10(12):1–18.
[42] Khosravi A. Design, analysis, and implementation of an integral terminal reduced order sliding mode controller for a self – lift positive output Luo converter via Filippov's technique considering the effects of parametric resistances. Int Trans Electr Energy Syst. 2018;29:1–33.
[43] Luo FL, Ye H. Advanced dc/dc converters. Boca Raton (FL): CRC Press; 2004.
[44] Andrew-Cotter J, Uddin MN, Amin IK. Particle swarm optimization based adaptive neuro-fuzzy inference system for MPPT control of a three-phase grid-connected photovoltaic system. 2019 IEEE International Electric Machines & Drives Conference (IEMDC); San Diego, CA, USA. 2019;2089–2094.